# fCUT&Tag-seq: An Optimized CUT&Tag-based Method for High-Resolution Histone Modification and Chromatin-Binding Protein Profiling in both Model and Plant Pathogenic Fungi

**Haiting Wang [1^], Yongjunlin Tan[2^], Jiayue Ma[1^], Jie Yang[1], Mengran Liu[1], Shan Lu[3], Haoxue Xia[4], Guangfei Tang[4], Wende Liu[4], Hui-Shan Guo[1*], Chun-Min Shan[1*]**

Affiliations:

1. State Key Laboratory of Plant Genomics, Institute of Microbiology, Chinese Academy of Sciences, Beijing, 100101, China
2. Shanxi Agricultural University, Taigu, 030800, China
3. College of Agriculture, Guangxi Key Laboratory of Sugarcane Biology, Guangxi University, Nanning, China
4. State Key Laboratory for Biology of Plant Diseases and Insect Pests, Institute of Plant Protection, Chinese Academy of Agricultural Sciences, Beijing 100193, China

^: contribute equally.

* E-mail: shancm@im.ac.cn (C.-M.S.); guohs@im.ac.cn (H.-S.G.);

E-mail and ORCID for all authors:

Haiting Wang > wanght@im.ac.cn, 0000-0003-3477-0217

Yongjunlin Tan >t17835090800@163.com, 0009-0007-1288-0147

Jiayue Ma > majiajia0529@gmail.com, 0009-0002-4644-1998

Jie Yang > yangjie@im.ac.cn, 0009-0003-9335-5803

Mengran Liu >liumr@im.ac.cn, 0009-0009-9946-6524

Shan Lu>lushan@gxu.edu.cn, 0000-0001-5368-896x

Haoxue Xia>xiahaoxue97@163.com, 0009-0000-4077-675X

Guangfei Tang>tangguangfei@caas.cn, 0000-0002-6999-6999

Wende Liu >liuwende@caas.cn, 0000-0002-5570-1395

Hui-Shan Guo > guohs@im.ac.cn, 0000-0002-3057-9303

Chun-Min Shan > shancm@im.ac.cn, 0000-0002-7080-5221

## Abstract

Histone modifications and chromatin-binding proteins are important regulators of gene expression in eukaryotes and have pivotal roles in fungal pathogenicity and development. However, profiling these modifications or proteins across the genome in fungi is still challenging, due to the technical limitations of the traditional widely-used ChIP-Seq method. Here, we present an optimized CUT&Tag-Seq protocol (fCUT&Tag-Seq) specifically designed for filamentous fungi and dimorphic fungi. Our approach involves the preparation of protoplasts and nuclear extraction to enhance antibody accessibility, along with formaldehyde crosslinking to improve protein-DNA binding efficiency. We then successfully applied fCUT&Tag-Seq to accurately profile multiple histone modifications like H3K9me3, H3K27me3, H3K4me3, and H3K18ac, across different plant pathogenic or model fungal species including *Verticillium dahliae*, *Neurospora crassa*, *Fusarium graminearum*, and *Sporisorium scitamineum*. Compared to the traditional ChIP-Seq, our method showed superior signal-to-noise ratios, higher reproducibility, and enhanced detection

sensitivity. Furthermore, we extended this method to profile chromatin-binding proteins, such as the histone acetyltransferase Gcn5. This study establishes fCUT&Tag-Seq as a robust and useful tool for fungal epigenetic research, enabling detailed exploration of chromatin dynamics and advancing our understanding of fungal gene regulation, development, and pathogenicity.

## Introduction

Chromatin structure and modifications are essential in regulating gene expression in eukaryotic organisms. The basic unit of chromatin, the nucleosome, consists of DNA wrapped around histone octamers composed of core histones H2A, H2B, H3, and H4[1]. The N-terminal tails of these histones can undergo various post-translational modifications (PTMs), such as methylation, acetylation, phosphorylation, ubiquitination, sumoylation, and ADP-ribosylation[2][3]. These modifications can alter chromatin structure and impact vital biological processes, such as gene expression, DNA repair, and chromosome organization**Error! Reference source not found.**[4].

Among these modifications, histone methylation is critical in regulating gene expression. For instance, trimethylation of histone H3 at lysine 9 (H3K9me3) and lysine 27 (H3K27me3) is highly associated with heterochromatin formation and gene silencing. In contrast, trimethylation of histone H3 at lysine 4 ( H3K4me3 ) , which typically occurs at transcription initiation sites, is commonly enriched near gene promoters and is associated with active transcription[6]-[8]. Furthermore, chromatin-binding proteins, such as the histone acetyltransferases and transcription factors, play crucial roles in modifying histones or binding to promoters, thus regulating gene expression, development, stress responses, and pathogenicity in eukaryotes, including fungi [9][10].

Traditional methods for studying histone modifications and chromatin-binding proteins have relied heavily on Chromatin Immunoprecipitation (ChIP) techniques, developed in the mid-1980s. The subsequent advent of ChIP followed by

high-throughput sequencing (ChIP-Seq) enables comprehensive identification of histone modification or protein-binding sites across the whole genome. While ChIP-Seq has become a foundational approach for genome-wide chromatin analysis, it still has several limitations. The method requires large amounts of input material, may suffer from epitope masking, and often produces high background noise with low signal-to-noise ratios[11]-[14]. These challenges are particularly pronounced when studying filamentous fungi, where rigid cell walls and secondary metabolites reduce antibody accessibility and affect immunoprecipitation efficiency[15].

The recent development of Cleavage Under Targets and Tagmentation (CUT&Tag) provids a more efficient method for profiling chromatin features[15]. This technique employs a tethered Tn5 transposase directed by specific antibodies to simultaneously cleave DNA at target sites and integrate sequencing adapters. CUT&Tag-Seq offers several advantages over traditional ChIP-Seq, including higher resolution mapping with lower cell input requirements (as few as 60 cells) and reduced background noise. While CUT&Tag has been successfully applied to mammalian, plant cells, and yeast, its application in filamentous fungi has been limited due to technical challenges posed by the fungal cell wall[17].

In this study, we present an optimized CUT&Tag-Seq method (fCUT&Tag-seq) adapted for plant pathogenic or model fungi, including various species such as *Verticillium dahliae*, *Neurospora crassa*, *Fusarium graminearum*, and *Sporisorium scitamineum*. Our study addresses the challenges posed by fungal cell walls through protoplast preparation and nuclear extraction, enhancing antibody accessibility and DNA availability. Additionally, for chromatin-binding proteins of low abundance, we incorporated a formaldehyde crosslinking step to strengthen protein-DNA interactions. We apply this method to diverse fungal species, focused on mapping the distribution of histone modifications (H3K9me3, H3K4me3, H3K27me3, and H3K18ac) and chromatin-binding proteins such as acetyltransferase SsGcn5. Our results demonstrate that the fCUT&Tag-Seq method can be successfully applied to filamentous fungi using low cell numbers, producing high-quality sequencing libraries with improved signal-to-noise ratios and reproducibility compared to traditional ChIP-Seq methods.

Implementing CUT&Tag-Seq in fungal studies offers a powerful tool for studying fungal epigenetics and gene regulation. This method reduces the required cell input and experimental duration, and enhances data quality, facilitating more detailed and accurate analyses of chromatin dynamics in fungi.

## Results

### Optimization and Implementation of CUT&Tag-Seq Method for Fungal Systems

We developed an optimized fCUT&Tag-Seq specifically adapted for fungal systems, building upon the traditional approach using the Vazyme Hyperactive Universal CUT&Tag Assay Kit for Illumina Pro (Cat. TD904). Our optimization addresses the unique challenges posed by fungal cell architecture while maintaining the high sensitivity and specificity characteristic of CUT&Tag methodology. The modified protocol incorporates several key steps for fungal applications **(Fig. 1).** To overcome the barrier presented by the fungal cell wall, we added a controlled enzymatic digestion step to generate protoplasts, followed by gentle nuclear extraction to preserve chromatin integrity. The isolated nuclei are then specifically captured by Concanavalin A-coated magnetic beads, which provide a stable platform for subsequent reactions while minimizing sample loss.

The workflow proceeds through several precisely controlled steps **(Fig. 1)**: (1) Nuclear membrane permeabilization is enhanced through carefully optimized digitonin treatment, facilitating antibody access while maintaining nuclear structural integrity. (2) Primary antibodies specific to the target histone modifications are introduced, followed by secondary antibodies that serve to amplify the detection signal. (3) The pA/G-Tn5 transferase complex is recruited to the antibody-bound locations through protein A/G interactions. (4) Upon $Mg^{2+}$ activation, the tethered Tn5 simultaneously cleaves adjacent DNA and integrates sequencing adapters, enabling efficient library preparation through subsequent PCR amplification. After library construction, next-generation sequencing and data analysis can be performed, to map the distribution pattern of histone modifications.

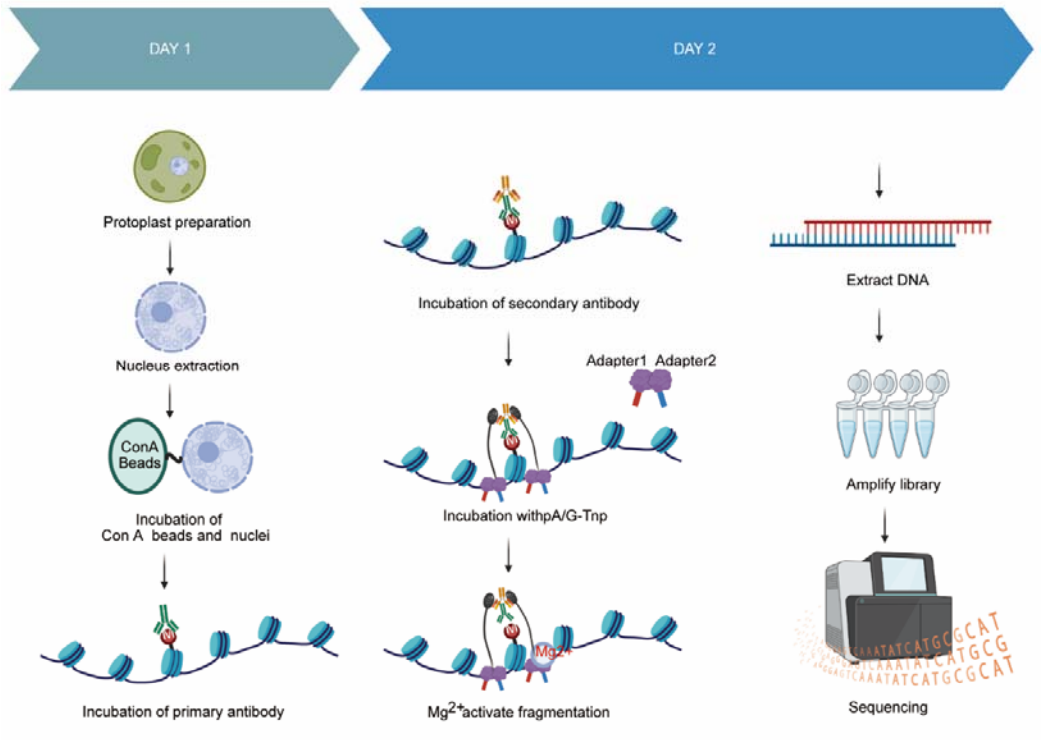


**Figure 1. Schematic overview of the fCUT&Tag-Seq workflow for filamentous fungi.**

Illustration of the key steps in the optimized fCUT&Tag-Seq protocol in filamentous fungi: (1) Preparation of fungal protoplasts through cell wall digestion; (2) Nuclear extraction from protoplasts; (3) Capture of nuclei using Concanavalin A-coated magnetic beads; (4) Addition of primary antibody specific to the histone modification or protein of interest; (5) Binding of secondary antibody; (6) Addition of pA/G-Tn5 transferase complex; (7) $Mg^{2+}$-activated DNA cleavage and adapter integration; (8) PCR amplification for library construction. The protocol incorporates digitonin treatment to enhance nuclear permeability and can be applied to both histone modification and chromatin-binding protein analysis.

## fCUT&Tag-Seq Demonstrates Superior Quality Control Metrics and Target Enrichment Compared to ChIP-Seq in *V. dahliae*

To evaluate if we could use fCUT&Tag-Seq for profiling histone modifications in filamentous fungi, we first selected the plant pathogenic fungus *V. dahliae* as a model system. This pathogenic fungus, known for its broad host range, causes severe wilt, yellowing, and vascular browning in infected plants, often resulting in significant crop losses[18]. Given the known roles of H3K9me3 and H3K27me3 in gene

155 silencing and pathogenicity [2][19], we focused our analysis on these two
156 modifications. To enhance our understanding of *V. dahliae*'s genetic background, we
157 sequenced the whole genome of *V. dahliae* V592 strain using Pacbio HiFi platform
158 **(Fig. S1)**. Using the genome of this specific strain as the reference for mapping can
159 avoid errors introduced by inter-species genomic differences, and also capture
160 species-specific epigenetic modifications of genes, thereby providing more accurate
161 information for following analyses.

162 We then compared traditional ChIP-Seq data from the SRA database (Home -
163 SRA - NCBI) and fCUT&Tag-Seq datasets based on multiple quality control metrics.
164 Initial quality control analysis of fCUT&Tag-Seq libraries revealed characteristic
165 nucleosomal ladder patterns through agarose gel electrophoresis, indicating successful
166 fragmentation and library preparation **(Fig. 2A)**. Fragment length distribution analysis
167 further confirmed the expected size distribution pattern typical of nucleosome-sized
168 fragments **(Fig. 2B)**, validating the technical success of our protocol. Comparative
169 analysis between fCUT&Tag-Seq and traditional ChIP-Seq demonstrated several key
170 advantages of our optimized method. Most notably, fCUT&Tag-Seq exhibited
171 significantly lower duplication rates (8.73%) compared to ChIP-Seq (88.45%),
172 indicating substantially improved library complexity and data utilization efficiency
173 **(Fig. 2C)**. Following alignment to the genome and subsequent filtering, we conducted
174 comprehensive quality metrics analysis using ChIPQC. The fCUT&Tag-Seq data
175 showed superior Signal Space Distance (SSD) scores, reflecting enhanced enrichment
176 efficiency. Furthermore, the Fraction of Reads in Peaks (FRiP) consistently exceeded
177 7.8% in fCUT&Tag-Seq samples, with H3K9me3 modification showing particularly
178 improved signal-to-noise ratios compared to ChIP-Seq **(Fig. 2D)**.Peak calling analysis
179 revealed comparable patterns between fCUT&Tag-Seq and ChIP-Seq data **(Fig. 2E**
180 **and 2F)**, validating the biological relevance of our results. However, CUT&Tag-seq
181 identified a greater number of peaks and showed improved signal intensity **(Fig. 2E)**,
182 indicating enhanced sensitivity and specificity in detecting histone modifications. The
183 improved signal-to-noise ratio was particularly evident in genome-wide coverage
184 plots, where fCUT&Tag-Seq showed more distinct enrichment patterns and clearer

peak boundaries **(Fig. 2F)**. These comprehensive quality metrics demonstrate that our fCUT&Tag-Seq protocol not only meets standard quality benchmarks but also offers superior performance compared to traditional ChIP-Seq methods in terms of data quality, enrichment efficiency, and technical reproducibility. The improved metrics suggest that this method provides a more reliable and efficient approach for studying histone modifications in *V. dahliae*.

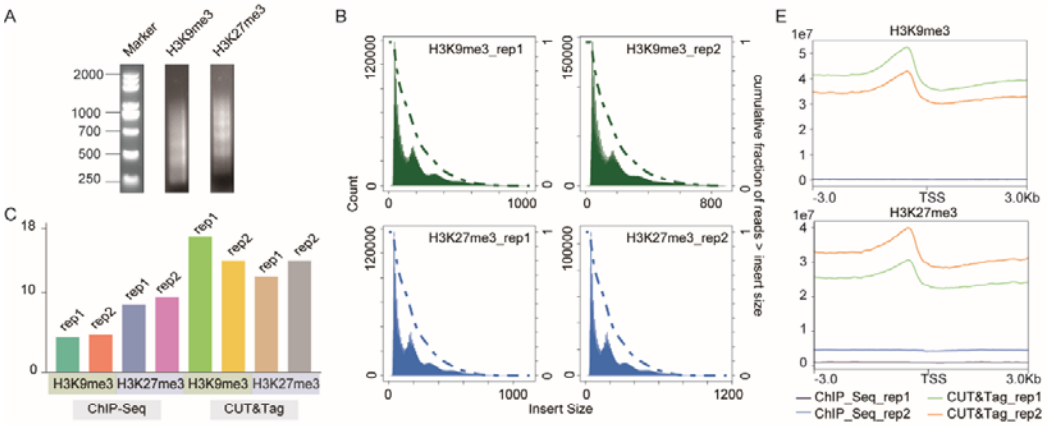


| Type | Sample | Fastp | | | ChipQC | | | |
|---|---|---|---|---|---|---|---|---|
| | | Raw Reads | After Filter | Dup% | Map% | Dup% | SSD | Frip% |
| ChIP_Seq | H3K9me3_rep1 | 9.266458M | 9.023016 M | 88.45% | 54 | 97 | 12 | 4.4 |
| | H3K9me3_rep2 | 12.815964 M | 12.435031 M | 88.06% | 55 | 96 | 12 | 4.7 |
| | H3K27me3_rep1 | 6.165582 M | 5.728879 M | 71.95% | 74 | 92 | 4.9 | 8.5 |
| | H3K27me3_rep2 | 10.090925 M | 9.397626 M | 60.14% | 84 | 81 | 5.6 | 9.4 |
| CUT&Tag | H3K9me3_rep1 | 24.473370 M | 24.179910 M | 8.62% | 84 | 20 | 8.6 | 14 |
| | H3K9me3_rep2 | 23.395988 M | 23.109170 M | 11.03% | 85 | 22 | 8.7 | 18 |
| | H3K27me3_rep1 | 21.760430 M | 21.506256 M | 7.85% | 90 | 22 | 15 | 12 |
| | H3K27me3_rep2 | 20.519482 M | 20.239132 M | 9.26% | 88 | 23 | 16 | 14 |

**Figure 2. Comprehensive quality control analysis of CUT&Tag-seq compared to ChIP-seq in *Verticillum dahliae*.**

**A.** Nucleosomal ladder pattern analysis of CUT&Tag-seq libraries by agarose gel electrophoresis. Libraries were generated from H3K9me3 and H3K27me3 histone modification profiling experiments in *Verticillum dahliae*. **B.** Fragment length distribution analysis of sequencing reads from fCUT&Tag-Seq and ChIP-Seq experiments. Green histograms represent H3K9me3 libraries (replicate 1 and replicate 2), while blue histograms show H3K27me3 libraries (replicate 1 and replicate 2). **C.** Bar plot representing the percentage of reads mapped to peak regions in the fCUT&Tag-Seq and ChIP-Seq datasets (rep1 and rep2). CUT&Tag had higher enrichment efficiency than ChIP-seq. **D.** Comparative analysis of key quality metrics between CUT&Tag-seq and ChIP-seq methods. Metrics include mapping rates (proportion of reads aligned to the reference genome), duplication rates (percentage of PCR

duplicates), and FRiP scores (Fraction of Reads in Peaks). Data demonstrate superior quality metrics for CUT&Tag-seq across all parameters. **E.** Signal intensity profiles across peaks in fCUT&Tag-Seq versus ChIP-Seq datasets, indicating higher signal-to-noise ratios in fCUT&Tag-Seq. The upper panel displays the H3K9me3 modification, while the lower panel shows the H3K27me3 modification. **F.** Genomic distribution analysis of identified peaks comparing CUT&Tag-Seq and ChIP-seq methods, showing increased sensitivity, specificity, lower background, and better repeatability in CUT&Tag-seq experiments. The displayed region is randomly selected. The upper panel represents the H3K9me3 modification, and the lower panel shows the H3K27me3 modification.

## fCUT&Tag-Seq Method Efficiently Profiles Histone Modifications in *V. dahliae*

Following validation of our optimized protocol, we applied fCUT&Tag-Seq to investigate the genome-wide distribution of two key repressive histone modifications, H3K9me3 and H3K27me3, in *V. dahliae*. To evaluate the specificity of our method, we analyzed both wild-type strains and their corresponding methyltransferase mutants (Vd*Δkmt1* and Vd*Δezh2)*. We incorporated spike-in controls for data normalization and used IgG antibodies as negative controls to account for background signal.

Genome-wide profiling revealed robust enrichment of both H3K9me3 and H3K27me3 modifications in wild-type strains **(Fig. 3A and 3B)**. In contrast, control experiments using non-specific IgG antibodies showed minimal signal across the genome, confirming the specificity of our approach **(Fig. S2A)**. Importantly, we observed significantly reduced levels of H3K9me3 and H3K27me3 in their respective methyltransferase mutants, Vd*Δkmt1* and Vd*Δezh2*, consistent with the loss of these enzymatic activities **(Fig. 3A and 3B)**.

Analysis of the genomic distribution of these modifications revealed distinct patterns. H3K9me3 peaks were predominantly located in promoter regions (68.81%) and intergenic spaces (25.28%), while H3K27me3 showed similar enrichment patterns with 87.56% of peaks in promoter regions and 8.58% in intergenic regions **(Fig. 3C)**. These distribution patterns align with the known roles of these modifications in transcriptional regulation. Comparison of signal intensities between fCUT&Tag-Seq and ChIP-Seq data demonstrated superior enrichment in CUT&Tag-seq experiments, particularly across gene bodies and their 3-kb flanking

regions **(Fig. S2B)**.

To assess the reproducibility of our modified protocol, we performed correlation analyses between biological replicates. fCUT&Tag-Seq demonstrated excellent reproducibility, with Pearson correlation coefficients of 0.99 and 1.0 for H3K9me3 and H3K27me3 modifications, respectively. These values exceeded those obtained from traditional ChIP-Seq experiments (0.91 and 0.89), highlighting the enhanced reliability of our optimized method **(Fig. 3D)**.

These results collectively demonstrate that our fCUT&Tag-Seq protocol enables highly specific and reproducible mapping of histone modifications in *V. dahliae*, providing a robust tool for investigating chromatin-based regulation in this important plant pathogen.

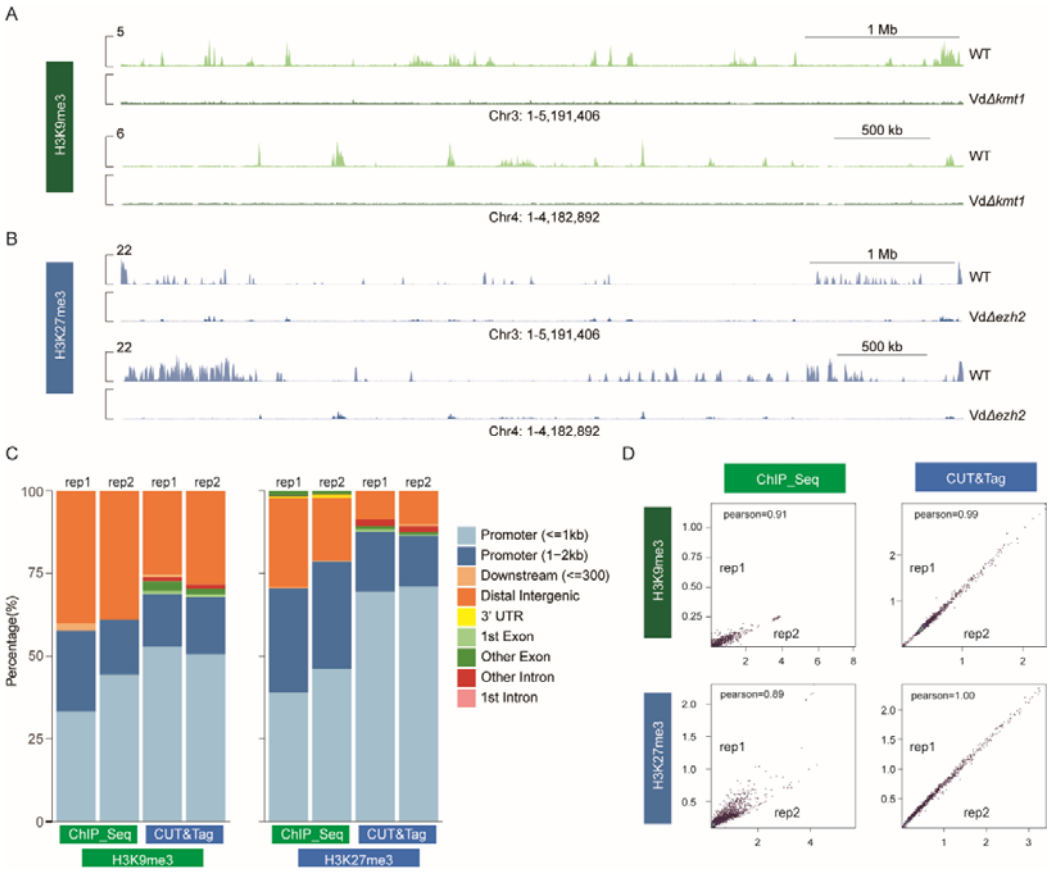


**Figure 3. Genome-wide profiling of histone modifications in *V. dahliae* using fCUT&Tag-seq**

**A.** Genome browser view of H3K9me3 distribution in wild-type and Vd*Δkmt1* strains. The tracks show specific H3K9me3 enrichment in WT and a significant reduction in the Vd*Δkmt1* mutant. **B.** Genome browser view of

H3K27me3 distribution in wild-type and Vd*Δezh2* strains. The tracks demonstrate specific H3K9me3 enrichment in WT and a significant reduction in the Vd*Δezh2* mutant. **C.** Comparative analysis of genomic feature distribution for H3K9me3 and H3K27me3 modifications between fCUT&Tag-seq and ChIP-seq approaches. The left panel shows the distribution of H3K9me3 peaks across different genomic elements, and the right panel shows H3K27me3 peak distribution, demonstrating the comprehensive coverage achieved by fCUT&Tag-seq. **D.** Pearson correlation analysis of signals between biological replicates for H3K9me3 and H3K27me3 modifications in CUT&Tag-seq (replicate 1 and replicate 2) and ChIP-seq experiments (replicate 1 and replicate 2). Pearson correlations were calculated using deepTools, with the multiBamSummary tool followed by plotCorrelation. Read counts were divided into 1,000-bp bins across the genome for the analysis. Higher correlation in CUT&Tag-seq showed better reproducibility.

## fCUT&Tag-Seq Method Shows Broad Applicability Across Model Filamentous Fungi

To assess whether our fCUT&Tag-seq protocol could be extended beyond *V. dahliae*, we tested it on two additional filamentous fungi: *N. crassa* and *F. graminearum*. Both species serve as valuable model organisms for studying fungal biology and pathogenicity, making them ideal candidates for validating broad applicability. Following the same experimental workflow, we focused on histone modifications H3K9me3 in *N. crassa*, and H3K4me3 in *F. graminearum*.

*N. crassa*, a member of the Ascomycota phylum, is widely recognized as a model organism due to its ease of cultivation and haploid genetics, which facilitate straightforward genetic analysis. Over the past few decades, it has been instrumental in studying various epigenetic modifications, including DNA methylation and gene silencing mechanisms[20][22]. We examined the levels of H3K9me3 in both the wild-type strain and the H3K9me3 methyltransferase mutant Nc*Δdim5*. Quality control assessments, including agarose gel electrophoresis and sequencing data analysis, confirmed that the fCUT&Tag-Seq libraries met the required standards **(Fig. 4A and 4B)**. The quality metrics indicated excellent performance for the *N. crassa* wild-type samples **(Fig. 4C)**. Notably, the peak distribution patterns observed were consistent with those identified through ChIP-Seq, yet CUT&Tag-Seq demonstrated

higher signal intensity. The correlation between CUT&Tag-Seq and ChIP-Seq data reached 0.73 **(Fig. 4D and 4E)**, further validating the reliability of our method. Additionally, biological replicates exhibited strong correlation, indicating high reproducibility **(Fig. 4F)**. Comparative analysis revealed that H3K9me3 was significantly enriched in the wild-type strain, while the Nc*Δdim5* mutant displayed markedly lower modification levels **(Fig. 4G)**. As expected, H3K9me3 modifications were predominantly located in distal intergenic regions and promoter regions **(Fig. 4H)**.

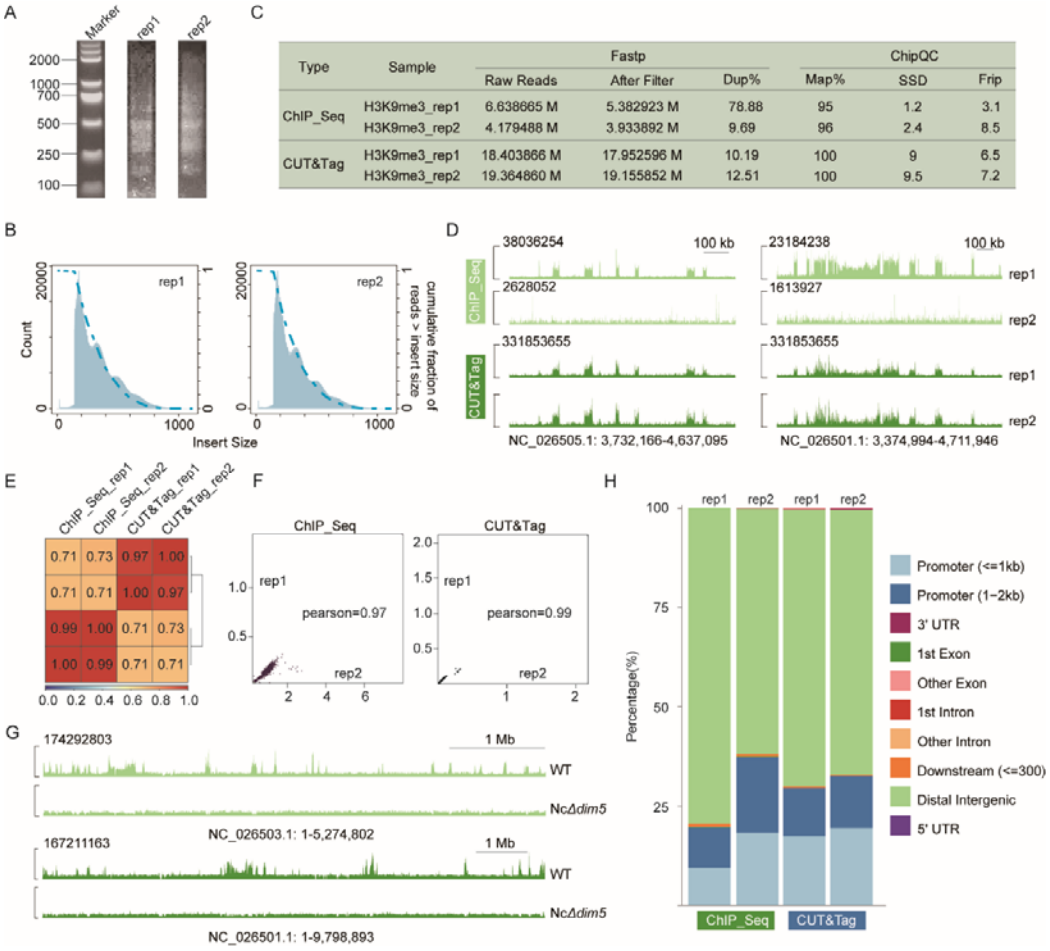


**Figure 4. Application of fCUT&Tag-seq for histone modification analysis in *N. crassa***

**A.** Nucleosomal ladder pattern analysis of fCUT&Tag-Seq libraries by agarose gel electrophoresis. Libraries were generated from two replicates of H3K9me3 profiling experiments in *N. crassa*. **B.** Fragment length distribution analysis of sequencing reads from fCUT&Tag-seq experiments. Histograms display the expected nucleosomal fragmentation patterns for 2 replicates. **C.** Comparative analysis between fCUT&Tag-Seq and ChIP-Seq data for

H3K9me3 modification in *N. crassa*. **D.** Genome browser view of peak distribution analysis comparing CUT&Tag-seq and ChIP-seq results. The upper panel shows H3K9me3 enrichment in ChIP-seq, and the lower panel displays the modification distribution from CUT&Tag-Seq. **E.** Correlation matrix analysis between CUT&Tag-Seq and ChIP-seq data, indicating strong agreement. Pearson correlations were calculated using deepTools (multiBamSummary followed by plotCorrelation), based on read counts divided into 1000-bp bins across the genome. **F.** Pearson correlation analysis of H3K9me3 signals between biological replicates in ChIP-Seq and fCUT&Tag-Seq, demonstrating higher reproducibility of fCUT&Tag-Seq. **G.** Genome browser view of the H3K9me3 peaks accross representative genomic regions in wild-type and Nc*Δdim5* strains in *N. crassa*. **H.** Feature distribution comparison of H3K9me3 modification between ChIP-seq and CUT&Tag-seq, showing similar distribution patterns between the two methods.

Similar results were obtained for *F. graminearum*, the causative agent of fusarium head blight in wheat [23]. In addition to analyzing H3K9me3 and H3K27me3 modifications, we also assessed H3K4me3 levels, which are associated with gene activation. The sequencing quality metrics of fCUT&Tag-Seq for *F. graminearum* were superior to those of ChIP-Seq, with a greater percentage of reads mapping to peak regions **(Fig. 5A and 5B)**. The Signal Space Distance (SSD) score and the percentage of reads in peaks (Rip%) reached 21 and 46, respectively **(Fig. 5B)**. These findings confirm the robustness of our method, as the wild-type strain exhibited significant enrichment **(Fig. 5C)**. Notably, peak enrichment was predominantly observed in the promoter regions (96.51%) **(Fig. 5D)**. And the Pearson correlation coefficient was 0.99, indicating a strong correlation between the sample groups **(Fig. 5E)**.

Overall, these results demonstrate that our fCUT&Tag-Seq method is not only effective for detecting histone modifications in *V. dahliae* but also applicable to other model fungi, including *N. crassa* and *F. graminearum*. This versatility underscores the potential of CUT&Tag-Seq as a powerful tool for studying epigenetic modifications across a broad range of fungal species.

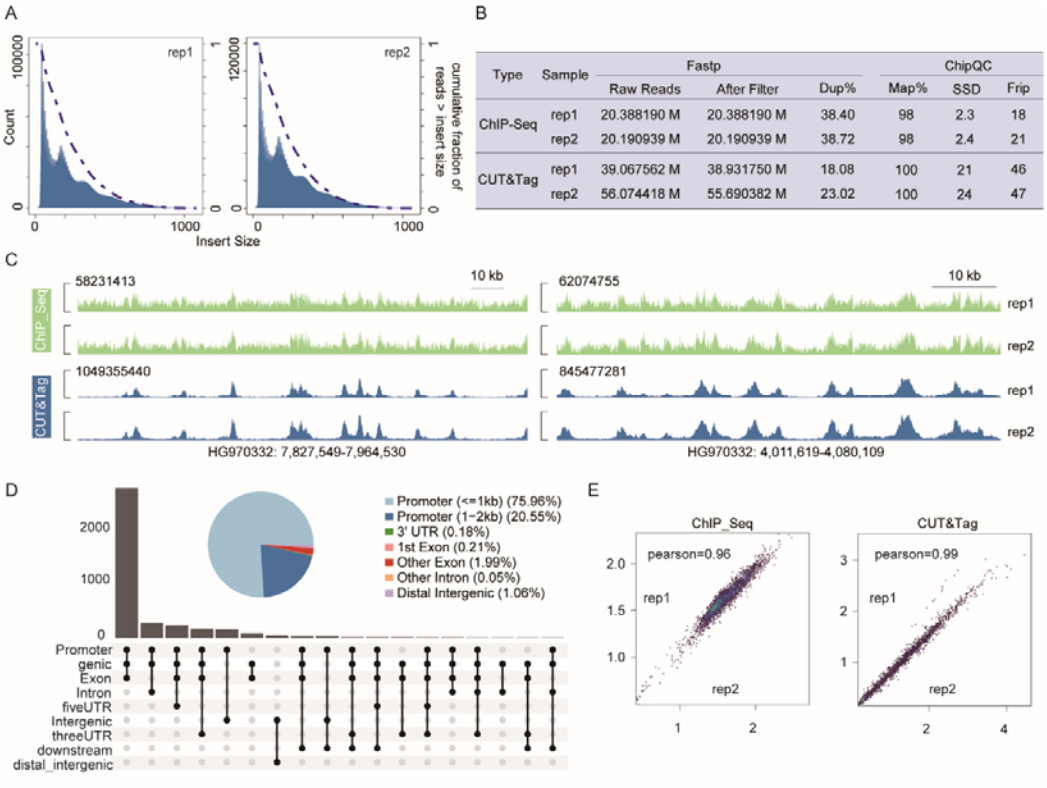


| Type | Sample | Fastp | | | ChipQC | | |
|---|---|---|---|---|---|---|---|
| | | Raw Reads | After Filter | Dup% | Map% | SSD | Frip |
| ChIP-Seq | rep1 | 20.388190 M | 20.388190 M | 38.40 | 98 | 2.3 | 18 |
| | rep2 | 20.190939 M | 20.190939 M | 38.72 | 98 | 2.4 | 21 |
| CUT&Tag | rep1 | 39.067562 M | 38.931750 M | 18.08 | 100 | 21 | 46 |
| | rep2 | 56.074418 M | 55.690382 M | 23.02 | 100 | 24 | 47 |

**Figure 5. Genome-wide profiling of H3K4me3 modifications in *F. graminearum* using fCUT&Tag-seq analysis**

**A.** Fragment length distribution of sequencing libraries for fCUT&Tag-Seq. The left panel shows the fragment length distribution for the H3K4me3 library in replicate 1, and the right panel shows the distribution for replicate 2. **B.** Comparative analysis of key quality metrics for ChIP-Seq and fCUT&Tag-Seq datasets, showing the higher quality of CUT&Tag-Seq. **C.** Genome browser view of H3K4me3 modification peak distribution analysis comparing fCUT&Tag-Seq and ChIP-Seq results. The genome regions were randomly selected. Green peaks represent ChIP-Seq results, and blue peaks represent CUT&Tag-Seq results. **D.** Genome browser view of the H3K4me3 peak distribution analysis comparing fCUT&Tag-Seq and ChIP-Seq results in two replicates of wild-type strain, showing significantly enrichment of H3K4me3 modification. **E.** The pie chart and UpSet plot illustrate the distribution of peaks across different genomic features. The results showing that H3K4me3 is predominantly enriched in promoter regions. Distinct colors represent different genomic features. **F.** Pearson correlation coefficients between sample groups for ChIP-Seq and fCUT&Tag-Seq, confirming high reproducibility for CUT&Tag-seq. The scatter plot displays normalized read counts in 1-kb bins across the genome.

## fCUT&Tag-Seq Method Also Enables Profiling of Chromatin-Binding Proteins

To extend the utility of our optimized CUT&Tag-Seq protocol beyond histone modifications, we adapted the method to profile chromatin-binding proteins, which play crucial roles in transcriptional regulation. Given the typically lower abundance of chromatin-binding proteins compared to histones, we incorporated an additional formaldehyde crosslinking step before protoplast preparation. This modification strengthens protein-chromatin interactions, thereby improving detection sensitivity. Following fragmentation, we performed sequential decrosslinking, protease digestion, and RNase treatment to ensure efficient DNA purification and library preparation **(Fig. 6)**.

To validate this adapted fCUT&Tag-seq method, we investigated the histone acetyltransferase Gcn5 in *S. scitamineum*, a dimorphic pathogenic fungus responsible for sugarcane smut. Sugarcane smut is one of the most significant diseases affecting global sugarcane production worldwide. The disease poses substantial economic threats, highlighting the urgent need for effective prevention and control strategies against *S. scitamineum*. It has been reported that histone acetylation may play a critical role in fungal pathogenesis [24][27]. To explore the relationship between histone acetylation and fungal pathogenicity, we screened possible histone acetyltransferase candidate genes and introduced a Flag epitope tag into the histone acetyltransferase Gcn5 in two *S. scitamineum* strains with different mating types (JG35 and JG36), employing our previously reported method [28].

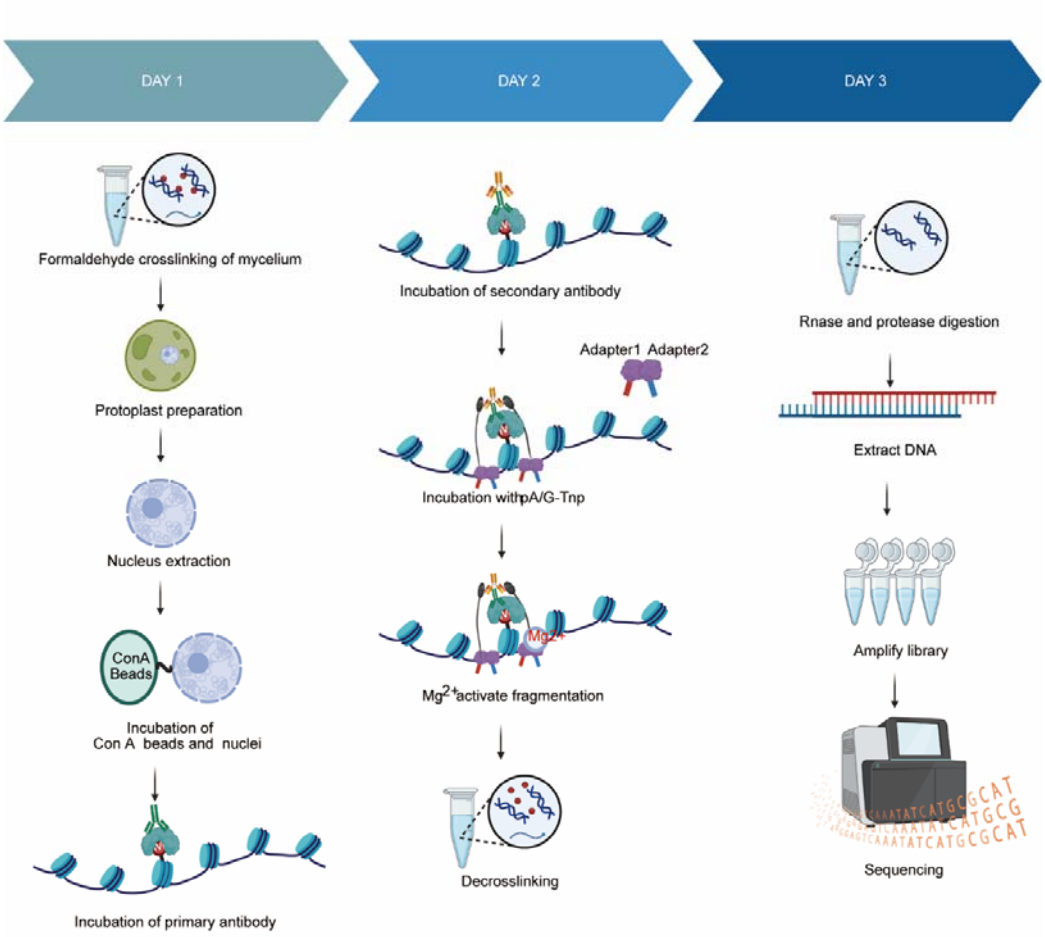


**Figure 6. Schematic overview of the optimized fCUT&Tag-seq method for detecting chromatin-binding proteins**

Workflow diagram illustrating the key steps of the fCUT&Tag-seq protocol for analyzing chromatin-binding proteins in fungi, including protoplast preparation, formaldehyde crosslinking, nuclear extraction, and subsequent CUT&Tag-Seq procedures.

Quality control analysis of the resulting CUT&Tag-Seq libraries revealed proper DNA fragmentation patterns by agarose gel electrophoresis and expected nucleosomal size distributions in sequencing reads **(Fig. 7A and 7B)**, confirming successful library preparation. Genome-wide profiling demonstrated robust enrichment of SsGcn5-3Flag binding sites across the *S. scitamineum* genome **(Fig. 7C and 7D)**. Notably, comparative analysis revealed a strong correlation between SsGcn5 binding sites and regions of H3K18 acetylation **(Fig. 7E)**, consistent with the known catalytic

activity of Gcn5. Feature distribution analysis showed that SsGcn5 binding sites were predominantly located in promoter regions (85.93% of total peaks) **(Fig. 7F)**, suggesting a primary role in transcriptional regulation. The high reproducibility of our method was demonstrated by the near-perfect Pearson correlation coefficient (approximately 1.0) between biological replicates **(Fig. 7G)**.

Our results confirmed that the fCUT&Tag-Seq method not only excels in detecting histone modifications, but also effectively profiles chromatin-binding proteins in filamentous fungi. By enhancing the detection of low-abundance proteins, this method also provides a powerful tool for exploring chromatin-binding proteins in regulating gene expression and chromatin dynamics across a broad range of fungal species.

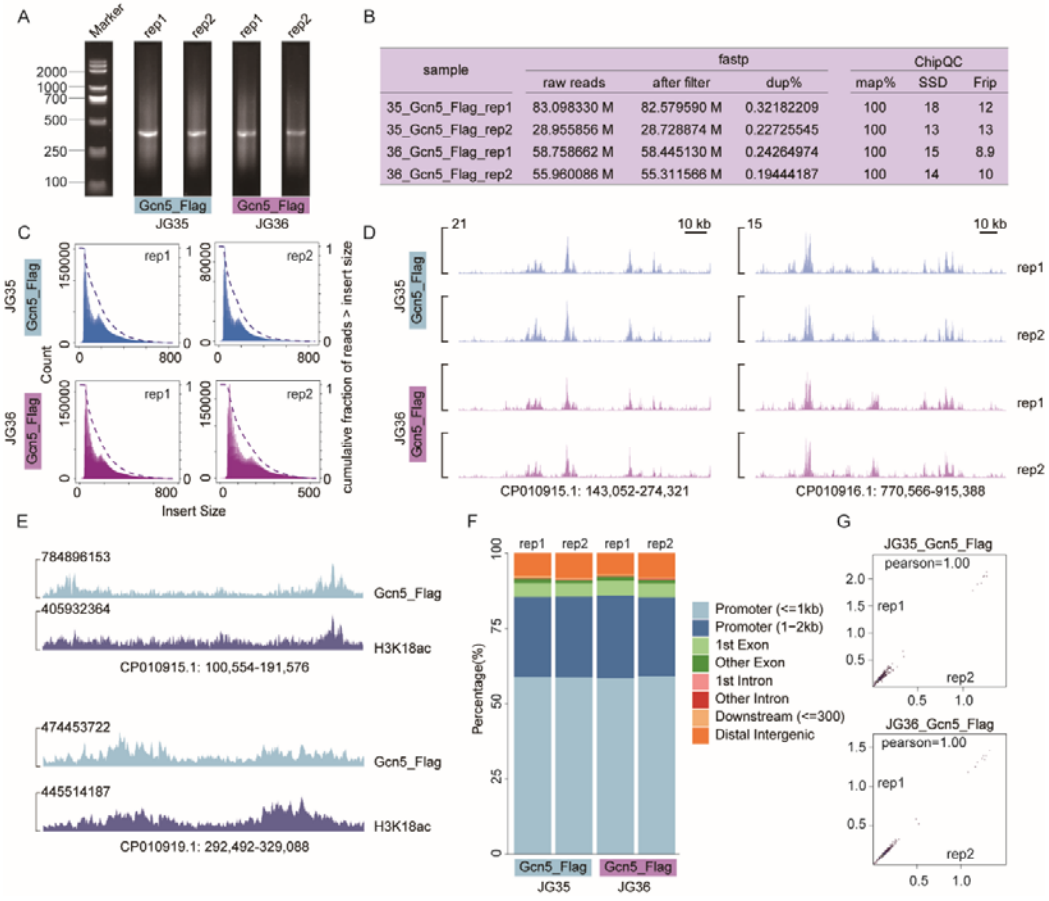


| sample | fastp | | | ChipQC | | |
|---|---|---|---|---|---|---|
| | raw reads | after filter | dup% | map% | SSD | Frip |
| 35_Gcn5_Flag_rep1 | 83.098330 M | 82.579590 M | 0.32182209 | 100 | 18 | 12 |
| 35_Gcn5_Flag_rep2 | 28.955856 M | 28.728874 M | 0.22725545 | 100 | 13 | 13 |
| 36_Gcn5_Flag_rep1 | 58.758662 M | 58.445130 M | 0.24264974 | 100 | 15 | 8.9 |
| 36_Gcn5_Flag_rep2 | 55.960086 M | 55.311566 M | 0.19444187 | 100 | 14 | 10 |

**Figure 7. Genome-wide profiling of SsGcn5 chromatin-binding protein and its correlation with H3K18ac modification in *S. scitamineum* using fCUT&Tag-seq**

**A.** Quality assessment of fCUT&Tag-seq libraries by agarose gel electrophoresis. DNA fragment distributions are

shown for two biological replicates of JG35 (lanes 1-2) and JG36 (lanes 3-4) mating types. **B.** Fragment length distribution analysis of sequencing reads demonstrating expected nucleosomal patterns. Blue and pink histograms represent Gcn5-Flag distributions in JG35 and JG36 strains, respectively. **C.** Comprehensive quality metrics for fCUT&Tag-seq datasets in DNA-binding protein enrichment in JG35 and JG36 strains. **D.** Genome browser view of SsGcn5-3Flag binding sites identified by CUT&Tag-Seq. Genome regions were selected randomly. **E.** Correlation analysis between SsGcn5-3Flag binding sites and H3K18ac modification regions, showing the functional relationship between histone acetyltransferase localization and its catalytic activity. **F.** Genomic feature distribution analysis of SsGcn5-Flag peaks in JG35 and JG36 strains, showing the relative enrichment across different genomic elements (promoters, gene bodies, intergenic regions). **G.** Correlation analysis between biological replicates for SsGcn5-3Flag CUT&Tag-seq experiments, demonstrating high reproducibility of the method.

## Conclusion & Discussion

Over prolonged evolutionary periods, plant pathogenic fungi have developed intricate strategies to penetrate and colonize their hosts. Precise control of pathogenic gene expression is pivotal to these infection processes, influencing fungal development, environmental stress responses, and virulence[29]. Emerging evidence underscores the importance of epigenetic regulation, including histone methylation, histone acetylation, and chromatin remodeling, in orchestrating such transcriptional reprogramming in plant pathogens[30]-[32]. However, until recently, the available tools for epigenetic research in diverse fungal systems were still very limited, making advanced investigations into fungal chromatin biology challenging.

CUT&Tag-Seq method, introduced by Kaya-Okur et al.[15] in 2019, offers a powerful alternative to ChIP-Seq through higher resolution and lower background noise. Yet its application had largely been confined to plant, yeast, and animal cells[15][33][34]. In this study, we optimized and extended CUT&Tag-Seq to several important fungal species, including *V. dahliae*, *F. graminearum*, *N. crassa*, and *S. scitamineum*. Our fCUT&Tag-Seq method effectively addresses the unique obstacles posed by fungal cell walls by integrating protoplast preparation and gentle nuclear

414 extraction. Additionally, a formaldehyde crosslinking step was introduced to
415 strengthen DNA-protein interactions, particularly beneficial for profiling
416 low-abundance chromatin-binding proteins.

417 Our data revealed that the fCUT&Tag-Seq method accurately and sensitively
418 detects histone modifications (H3K9me3, H3K27me3, H3K4me3, and H3K18ac) as
419 well as chromatin-binding proteins in these fungi. Furthermore, our comparisons with
420 conventional ChIP-Seq protocols highlighted notable improvements in library
421 complexity, signal-to-noise ratios, and correlation across biological replicates. These
422 advantages facilitate comprehensive insights into the epigenetic landscapes governing
423 fungal pathogenicity, development, and physiology.

424 While our fCUT&Tag-Seq method has demonstrated significant improvements
425 in data quality and sensitivity, it is important to acknowledge the limitations.
426 Challenges remain in enriching low-abundance proteins and chromatin-binding
427 proteins located at the heterochromatin regions, where the antibody accessibilities are
428 largely reduced. Future studies should focus on further optimizing methods for
429 relaxing heterochromatin to enhance the detection of these proteins.

430 Taken together, we established fCUT&Tag-Seq as a robust and versatile method
431 for fungal epigenetic research. By reducing cell input requirements and enhancing
432 data quality, it enables a deeper exploration of chromatin-based mechanisms that
433 shape fungal behavior and plant-fungus interactions. We anticipate that future studies
434 will leverage this method to uncover new regulatory pathways, thereby advancing the
435 characterization of fungal pathogenicity and guiding innovative approaches for crop
436 disease management.

437

438 **Materials and Methods**

439 **Fungal Strains and Culture Conditions**

440 The following fungal strains were used in this study: *V. dahliae* strain V592 (isolated
441 from cotton in Xinjiang, China) [35][36], *N. crassa* 87-3 and Nc*Δdim5* (provided by
442 Xiao Liu)[37], *S. scitamineum* strains JG35 and JG36 (provided by Shan Lu)[38], and

*F. graminearum* wild-type strain (provided by Guangfei Tang and Haoxue Xia)[39]. All strains were maintained and cultured according to standard protocols specific to each species.

**Generation of Mutant and Tagged Fungal Strains**

For *V. dahliae*, *VdKMT1* (*VDAG_07826*) and *VdEZH2* (*VDAG_00983*) deletion strains (Vd*Δkmt1* and Vd*Δezh2*) were constructed as previously reported[40]. 1kb genomic sequences upstream and downstream of target genes were amplified from V592 DNA with the following primer pairs: VdKMT1-A/ VdKMT1-a, VdKMT1-d/ VdKMT1-B, VdEZH2-A/ VdEZH2-a, VdEZH2-d/ VdEZH2-B (listed in Table S1) using the Phanta Max Super-Fidelity DNA Polymerase (P505, Vazyme) and cloned into the pGKO-HPT / pGKO-NAT vector *via* homologous recombination. Sequence-verified vectors were then used to transform *V. dahliae* by *Agrobacterium tumefaciens*-mediated transformation (ATMT) system. *V. dahliae* transformants were selected on potato dextrose agar (PDA) plates supplemented with 5-fluoro-2'deoxyuridine (5FU) and hygromycin B / Nourseothricin. Putative transformants were screened utilizing PCR to confirm the successful deletion of target genes by primer pairs: V1/Hpt-R and V2/Hpt-F. The primers used in construction are listed in Table S1.

For *S. scitamineum*, the SsGcn5-3Flag strain was constructed using homologous recombination. The engineered vector pEX1-GAP-Flag-HPT, which carries a Flag tag, was initially constructed by modifying the pEX1-GAP-HPT vector. Subsequently, approximately 1.5 kb of upstream (5') and downstream (3') flanking sequences near the target protein's stop codon, excluding the stop codon itself, were amplified using PCR from the wildtype strains JG35 and JG36 with the following primer pairs: SsGcn5-tg-A/SsGcn5-a, SsGcn5-d/SsGcn5-B (listed in Table S1). Furthermore, two truncated fragments of the hygromycin resistance gene HPT, designated HPT-up and HPT-down, were amplified from the pEX1-GAP-Flag-HPT plasmid via PCR with the following primer pairs: HPT-LB-F/HPT-LB-R, HPT-RB-F/HPT-RB-R. Overlap PCR was employed to fuse the upstream DNA sequence with HPT-up with the primer pair

SsGcn5-tg-A/ HPT-LB-R and the downstream DNA sequence with HPT-down with the primer pair HPT-RB-F/ SsGcn5-B, and the products were introduced into *S. scitamineum* strains JG35 and JG36 using PEG-mediated protoplast transformation. Transformants were selected on YEPSA medium containing 150 μg/mL hygromycin B and verified by PCR using primer pairs SsGcn5-C(V1)/Hpt-LB-R and SsGcn5-D(V2)/Hpt-RB-F.

**fCUT&Tag-Seq for Histone Modification**

To detect histone modifications using CUT&Tag-Seq, protoplasts were first prepared. This was achieved by digesting mycelium (*V. dahliae*, *N. crassa* and *F. graminearum*) or spores (*S. scitamineum*) with 10 mL of enzyme solution (0.25g VinoTaste®Pro enzyme is dissolved in 12.5 mL 0.7 M NaCl for *V. dahliae*, *N. crassa* and *S. scitamineum*'s protoplasts preparation; 0.1 g Diselease, 0.2 g Celulase and 0.2 g Lysozyme were diluted with 0.7 M NaCl to 20 mL for *F. graminearum*'s protoplasts preparation). The requisite digestion time was contingent upon the specific fungus, with the following durations observed: 3 h for *V. dahliae* mycelium, *F. graminearum* and *N. crassa* mycelium, and 30 min for *S. scitamineum* spores. Filtering protoplasts with Miracloth (475855-1R; Merck), followed by centrifugation for 10 min at 3800 rpm for *V. dahliae* and *N. crassa*, 2200 rpm for *S. scitamineum* and 5000 rpm for *F. graminearum*, 25□. Protoplasts were resuspended using 10 mL of 0.7 M NaCl, collected by centrifugation. Finally, the number of cells was counted using a hemocytometer.

For extracting nuclei, take 1 million cells for 1.5 mL EP tubes based on the number of cells counted, followed by centrifugation at 3000 rpm at 25□ for 5 min. The precipitate was resuspended with 100 μL of nuclear extract buffer (TD904; Vazyme) and left on ice for 10 min, followed by centrifugation at 2500 rpm at 25□ for 6 min. Carefully remove the supernatant and resuspend the nuclei by adding 100 μL of wash buffer (TD904; Vazyme).

For the adsorption of nuclei, activated Concanavalin A-coated magnetic beads (TD904; Vazyme) and 250,000 resuspended cell nuclei were added to 200 μl 8-row tubes, along with 75 μl of wash buffer (TD904; Vazyme). The contents were then

503 mixed by inverting the tubes. Leave at room temperature for 10 min, turning up and
504 down 2-3 times.

505 In setting up for the antibody reaction, the 8-row tubes from the previous step
506 were placed on a magnetic rack, the 8-row tubes were removed after discarding the
507 supernatant, and 50 μL of antibody buffer (TD904; Vazyme) was added to each
508 sample to resuspend the magnetic bead cell nuclear complex. Add 1 μL of antibody
509 against trimethylation of histone 3 at lysine 9 (H3K9me3) (Cat39161; Active Motif),
510 trimethylation of histone 3 at lysine 27 (H3K27me3) (Cat39155; Active Motif), and
511 trimethylation of histone 3 at lysine 4( H3K4me3 )(Cat39060; Active Motif) according
512 to the ratio used. After mixing upside down and upside down, centrifuge instantly and
513 place in the refrigerator at 4°C overnight.

514 On the second day, the overnight magnetic bead antibody complexes were
515 mixed upside down and centrifuged instantaneously before being placed on a
516 magnetic rack. After clarifying and discarding the supernatant, 0.5 μL of rabbit
517 antibody (Ab207; Vazyme) was mixed with 49.5 μL of Dig wash buffer (792 μL Wash
518 Buffer, 8 μL 5% Digitonin) and added to each sample, which was slowly spun for 1 h
519 at room temperature (9-11 rpm/min). After transient centrifugation on a magnetic rack,
520 the supernatant was clarified and discarded and the beads was washed three times
521 with 200 μL of Dig wash buffer.

522 For transposase incubation, 2 μL of Hyperactive pA/G-Transposon (TD904;
523 Vazyme) in 98 μL Dig-300 buffer (100 μL 10 × Dig-300 Buffer, 2 μL 5% Digitonin,
524 20 μL 50×protease inhibitor, 878 μL dd$H_2O$) was added to each reaction and
525 incubated with gentle rotation (9-11 rpm/min) at room temperature for 1 h.
526 Subsequently, instantaneous centrifugation on a magnetic rack, clarification and
527 discarding of supernatant, and wash three times using 200 μL Dig-300 buffer to
528 remove unbound pA/G-Transposon.

529 For fragmentation, 10 μL trueprep tagment buffer L (TD904; Vazyme) in 40 μL
530 Dig-300 buffer was added to each reaction and incubated at 37°C for 1 h.

531 For DNA extraction, 2 μL 10% SDS (TD904; Vazyme) was added to stop the

fragmentation reaction, and 0.5 μL DNA spike in (TD904; Vazyme) was added as a reference standard between samples during sequencing, after mixing, 55°C for 10 min. Instantaneous centrifugation was placed on a magnetic rack and the supernatant was transferred to a new 200 μL 8-row tube. Add 50 μL the activated DNA extract beads (TD904; Vazyme) to the 8-row tube containing the supernatant, mix upside down, and incubate for 20 min at room temperature, mixing 2-3 times during the incubation. Instantaneous centrifugation, 8-row tubes were placed on a magnetic rack, clarified by discarding the supernatant, washed twice with 200 μL of 1x B&W buffer (TD904; Vazyme), dried on a magnetic rack, and resuspended the magnetic bead DNA complex by adding 30 μL of RNAase free dd$H_2O$.

Libraries for deep sequencing were constructed by PCR, with the PCR reaction (50 μL) set up as follows:15 μL beads with affinity purified DNA, 25 μL 2xCUT&Tag Amplification Mix (TD904; Vazyme), 5 μL N5XX Primer (TD202; Vazyme), 5 μL N7XX Primer (TD202; Vazyme). The adaptor pooling guide strategy from Illumina was followed. Each PCR solution was mixed gently blowing with a pipette. Denaturation: 72°C for 3 min, 95°C for 3 min; Cycling reaction: 98°C for 10 s, 60°C for 5 s; Extension: 72°C for 1 min, 4°C hold. The number of cycles of the PCR reaction ranged from 9 to 20.

For PCR product purification, 100 μL of VAHTS DNA clean beads (N411; Vazyme) were added to the 8-row tube where the PCR reaction was completed. Mix by vortex oscillation and let stand at room temperature for 5 min. Centrifuge the 8-row tube on a magnetic rack, clarify and discard the supernatant, wash twice with 200 μL of 80% ethanol, dry on the magnetic rack, add 22 μL of RNAase-free dd$H_2O$ to resuspend the magnetic beads PCR product complex, and incubate for 5 min at room temperature. Place on a magnetic rack for clarification, and transfer supernatant to a new 1.5 mL EP tube. Followed by quality control and deep sequencing.

**fCUT&Tag-Seq for chromatin-binding protein proteins**

To analyze lower-abundance chromatin-binding proteins, such as transcription factors or histone acetyltransferases, a formaldehyde crosslinking step was integrated.

Approximately 1 g of fungal spores was fixed with 9 mL 0.1% formaldehyde for 8 min at room temperature. The cross-linking was subsequently stopped by 1 mL of 2 M glycine for 5 min at room temperature. The cross-linked cells were washed three times using 20 mL SCS buffer.

Following crosslinking, protoplast formation and nuclei capture with ConA-beads were performed as described above. After incubation with the appropriate chromatin-binding protein antibodies, the pA/G-Tn5 transposome was assembled onto the antibody-bound locus. DNA extraction, and purification were carried out similarly to the procedure for histone modifications. To reverse crosslinks, samples were incubated overnight at 65°C with 3 μL 5 M NaCl. RNA was removed by RNase A treatment (37°C for 30 min), and proteins were digested by Proteinase K (incubation at 53°C for 1 h). Proteases were removal by protease inhibitors (room temperature for 5 min). Purified DNA libraries were further processed by PCR amplification.

**CUT&Tag-seq Data Analysis**

Raw ChIP-seq data were downloaded from the SRA database using SRA Toolkit (3.1.1). Raw data of ChIP-seq and CUT&Tag were first processed using fastp (0.23.4) [41] to remove adapters and low-quality sequences. The cleaned reads were then aligned to the spike-in sequences using BWA (0.7.18) [42]. After alignment, samtools (1.21) [43] was used to count the number of successfully mapped reads. The sample with the fewest mapped reads was selected as the baseline for spike-in normalization. The normalized data were then re-aligned to the reference genome using BWA (0.7.18), with reads having a quality score below 20 being filtered out using samtools (1.21). The alignment results were then processed using Picard (Picard Tools - By Broad Institute) for sorting and deduplication. Peak calling was performed using MACS2 (2.2.9.1) [44], with IgG controls used to correct for background. The "-B" flag was employed to generate histone modification and control lambda .bdg files, which were subsequently compared using the bdgcmp function in MACS2. ChIPQC (1.42.0, Bioconductor - ChIPQC) was applied for quality control of the CUT&Tag

analysis. Graphical representations of the data were generated using Spark.py (2.6.2) [45]. Peak annotation was performed using ChIPseeker (1.42.0) [46] to assign genomic features to the identified peaks. Correlation analysis was carried out using the multiBigwigSummary and plotCorrelation functions of deepTools (3.3.5) [47], while heatmaps were generated using the computeMatrix and plotHeatmap functions of deepTools (3.3.5).

## Data Availability

All ChIP-seq data were obtained from the SRA database (Home - SRA - NCBI). The ChIP-seq data for H3K9me3 modification in *V. dahliae* were downloaded from SRR10571946 and SRR10571947, respectively, and data for H3K27me3 modification were downloaded from SRR10571948 and SRR10571949. For H3K9me3 modification in *N. crassa*, the ChIP-seq data were downloaded from SRR1566112 and SRR12229310. The ChIP-seq data for H3K4me3 modification in *F. graminearum* were downloaded from SRR21677668 and SRR21677669. The reference genomes used in the mapping process are as follows: PRJNA1212841 for *V. dahliae* V592, GCF_000182925.2 for *N. crassa*, FgraminearumPH-1 for *F. graminearum* (available at FungiDB), and GCA_001010845.1 for *S. scitamineum*. The CUT&Tag data used in this study are available in the NCBI BioProject database under accession number PRJNA1213569 and PRJNA1166993.

## References

[1] Luger, K., Mäder, A. W., Richmond, R. K., Sargent, D. F., & Richmond, T. J. (1997). Crystal structure of the nucleosome core particle at 2.8 A resolution. *Nature*, *389*(6648), 251–260.

[2] Kouzarides T. (2007). Chromatin modifications and their function. *Cell*, *128*(4), 693–705.

[3] Allis, C. D., & Jenuwein, T. (2016). The molecular hallmarks of epigenetic control. *Nature reviews. Genetics*, *17*(8), 487–500.

[4] Zhang, Y., Sun, Z., Jia, J., Du, T., Zhang, N., Tang, Y., Fang, Y., & Fang, D. (2021). Overview of Histone Modification. *Advances in experimental medicine and biology*, *1283*, 1–16.

[5] Strahl, B. D., & Allis, C. D. (2000). The language of covalent histone modifications. *Nature*, *403*(6765), 41–45.

[6] Lachner, M., O'Carroll, D., Rea, S., Mechtler, K., & Jenuwein, T. (2001). Methylation of histone H3 lysine 9 creates a binding site for HP1 proteins. *Nature*, *410*(6824), 116–120.

[7] Schuettengruber, B., Bourbon, H. M., Di Croce, L., & Cavalli, G. (2017). Genome Regulation by Polycomb and Trithorax: 70 Years and Counting. *Cell*, *171*(1), 34–57.

[8] Wang, H., Fan, Z., Shliaha, P. V., Miele, M., Hendrickson, R. C., Jiang, X., & Helin, K. (2023). H3K4me3 regulates RNA polymerase II promoter-proximal pause-release. *Nature*, *615*(7951), 339–348.

[9] Chen, M., Liu, Y., Liu, Z., Su, L., Yan, L., Huang, Y., Huang, Y., Zhang, W., Xu, X., & Zheng, F. (2023). Histone acetyltransferase Gcn5-mediated histone H3 acetylation facilitates cryptococcal morphogenesis and sexual reproduction. *mSphere*, *8*(6), e0029923.

[10] Shivarathri, R., Tscherner, M., Zwolanek, F., Singh, N. K., Chauhan, N., & Kuchler, K. (2019). The Fungal Histone Acetyl Transferase Gcn5 Controls Virulence of the Human Pathogen Candida albicans through Multiple Pathways. *Scientific reports*, *9*(1), 9445.

[11] Park P. J. (2009). ChIP-seq: advantages and challenges of a maturing technology. *Nature reviews. Genetics*, *10*(10), 669–680.

[12] Furey T. S. (2012). ChIP-seq and beyond: new and improved methodologies to detect and characterize protein-DNA interactions. *Nature reviews. Genetics*, *13*(12), 840–852.

[13] Locke, G., Haberman, D., Johnson, S. M., & Morozov, A. V. (2013). Global remodeling of nucleosome positions in C. elegans. *BMC genomics*, *14*, 284.

[14] Dahl, J. A., & Collas, P. (2008). A rapid micro chromatin immunoprecipitation

650 assay (microChIP). *Nature protocols*, *3*(6), 1032–1045.

651 [15] Torres-Garcia, S., Huang, Y., Dewornu, F. S., Tong, P., Yeboah, R., Allshire, R., &
652 Shukla, M. (2025). Genome-Wide Profiling of Histone Modifications in Fission
653 Yeast Using CUT&Tag. *Methods in molecular biology (Clifton, N.J.)*, *2862*,
654 309–320.

655 [16] Kaya-Okur, H. S., Wu, S. J., Codomo, C. A., Pledger, E. S., Bryson, T. D.,
656 Henikoff, J. G., Ahmad, K., & Henikoff, S. (2019). CUT&Tag for efficient
657 epigenomic profiling of small samples and single cells. *Nature*
658 *communications*, *10*(1), 1930.

659 [17] Liu, Y., Siejka-Zielińska, P., Velikova, G., Bi, Y., Yuan, F., Tomkova, M., Bai, C.,
660 Chen, L., Schuster-Böckler, B., & Song, C. X. (2019). Bisulfite-free direct
661 detection of 5-methylcytosine and 5-hydroxymethylcytosine at base
662 resolution. *Nature biotechnology*, *37*(4), 424–429.

663 [18] Klosterman, S. J., Atallah, Z. K., Vallad, G. E., & Subbarao, K. V. (2009).
664 Diversity, pathogenicity, and management of verticillium species. *Annual review*
665 *of phytopathology*, *47*, 39–62.

666 [19] Studt-Reinhold, L., Atanasoff-Kardjalieff, A. K., Berger, H., Petersen, C.,
667 Bachleitner, S., Sulyok, M., Fischle, A., Humpf, H. U., Kalinina, S., &
668 Søndergaard, T. E. (2024). H3K27me3 is vital for fungal development and
669 secondary metabolite gene silencing, and substitutes for the loss of H3K9me3 in
670 the plant pathogen Fusarium proliferatum. *PLoS genetics*, *20*(1), e1011075.

671 [20] Aramayo, R., & Selker, E. U. (2013). Neurospora crassa, a model system for
672 epigenetics research. *Cold Spring Harbor perspectives in biology*, *5*(10), a017921.

673 [21] Honda, S., Lewis, Z. A., Huarte, M., Cho, L. Y., David, L. L., Shi, Y., & Selker, E.
674 U. (2010). The DMM complex prevents spreading of DNA methylation from
675 transposons to nearby genes in Neurospora crassa. *Genes & development*, *24*(5),
676 443–454.

677 [22] Chicas, A., Cogoni, C., & Macino, G. (2004). RNAi-dependent and

678 RNAi-independent mechanisms contribute to the silencing of RIPed sequences in
679 Neurospora crassa. *Nucleic acids research*, *32*(14), 4237–4243.
680 [23] Kim, J. E., Nam, H., Park, J., Choi, G. J., Lee, Y. W., & Son, H. (2020).
681 Characterization of the CCAAT-binding transcription factor complex in the plant
682 pathogenic fungus Fusarium graminearum. *Scientific reports*, *10*(1), 4898.
683 [24] Elías-Villalobos, A., Fernández-Álvarez, A., Moreno-Sánchez, I., Helmlinger, D.,
684 & Ibeas, J. I. (2015). The Hos2 Histone Deacetylase Controls Ustilago maydis
685 Virulence through Direct Regulation of Mating-Type Genes. *PLoS*
686 *pathogens*, *11*(8), e1005134.
687 [25] Hou, X., Liu, L., Li, Y., Wang, P., Pan, X., Xu, D., Lai, D., & Zhou, L. (2024).
688 Regulation of Histone Acetylation Modification on Biosynthesis of Secondary
689 Metabolites in Fungi. *International journal of molecular sciences*, *26*(1), 25.
690 [26] Su, C., Lu, Y., & Liu, H. (2016). N-acetylglucosamine sensing by a GCN5-related
691 N-acetyltransferase induces transcription via chromatin histone acetylation in
692 fungi. *Nature communications*, *7*, 12916.
693 [27] Zhang, S., Guo, Y., Li, S., & Li, H. (2022). Histone Acetyltransferase
694 CfGcn5-Mediated Autophagy Governs the Pathogenicity of *Colletotrichum*
695 *fructicola*. *mBio*, *13*(5), e0195622.
696 [28] Yang, J., Liu, M., Jiao, Y., Guo, H. S., Shan, C. M., & Wang, H. (2024). An
697 Efficient Homologous Recombination-Based In Situ Protein-Labeling Method
698 in *Verticillium dahliae*. *Biology*, *13*(2), 81.
699 [29] John, E., Singh, K. B., Oliver, R. P., & Tan, K. C. (2021). Transcription factor
700 control of virulence in phytopathogenic fungi. *Molecular plant pathology*, *22*(7),
701 858–881.
702 [30] Millán-Zambrano, G., Burton, A., Bannister, A. J., & Schneider, R. (2022).
703 Histone post-translational modifications - cause and consequence of genome
704 function. *Nature reviews. Genetics*, *23*(9), 563–580.

[31] Collemare, J., & Seidl, M. F. (2019). Chromatin-dependent regulation of secondary metabolite biosynthesis in fungi: is the picture complete?. *FEMS microbiology reviews*, *43*(6), 591–607.

[32] Kang, H., Fan, T., Wu, J., Zhu, Y., & Shen, W. H. (2022). Histone modification and chromatin remodeling in plant response to pathogens. *Frontiers in plant science*, *13*, 986940.

[33] Tao, X. Y., Guan, X. Y., Hong, G. J., He, Y. Q., Li, S. J., Feng, S. L., Wang, J., Chen, G., Xu, F., Wang, J. W., & Xu, S. C. (2023). Biotinylated Tn5 transposase-mediated CUT&Tag efficiently profiles transcription factor-DNA interactions in plants. *Plant biotechnology journal*, *21*(6), 1191–1205.

[34] Kaya-Okur, H. S., Janssens, D. H., Henikoff, J. G., Ahmad, K., & Henikoff, S. (2020). Efficient low-cost chromatin profiling with CUT&Tag. *Nature protocols*, *15*(10), 3264–3283.

[35] Gao, F., Zhou, B. J., Li, G. Y., Jia, P. S., Li, H., Zhao, Y. L., Zhao, P., Xia, G. X., & Guo, H. S. (2010). A glutamic acid-rich protein identified in Verticillium dahliae from an insertional mutagenesis affects microsclerotial formation and pathogenicity. *PloS one*, *5*(12), e15319.

[36] Liu, Q., Li, Y., Wu, H., Zhang, B., Liu, C., Gao, Y., Guo, H., & Zhao, J. (2023). Hyphopodium-Specific Signaling Is Required for Plant Infection by *Verticillium dahliae*. *Journal of fungi (Basel, Switzerland)*, *9*(4), 484.

[37] Liu, X. L., Yang, Y., Hu, Y., Wu, J., Han, C., Lu, Q., Gan, X., Qi, S., Guo, J., He, Q., Liu, Y., & Liu, X. (2023). The nutrient-sensing GCN2 signaling pathway is essential for circadian clock function by regulating histone acetylation under amino acid starvation. *eLife*, *12*, e85241.

[38] Lu, S., Wang, Y., Shen, X., Guo, F., Zhou, C., Li, R., & Chen, B. (2021). SsPEP1, an Effector with Essential Cellular Functions in Sugarcane Smut Fungus. *Journal of fungi (Basel, Switzerland)*, *7*(11), 954.

[39] Tang, G., Xia, H., Huang, Y., Guo, Y., Chen, Y., Ma, Z., & Liu, W. (2024). Liquid-liquid phase separation of H3K27me3 reader BP1 regulates transcriptional repression. *Genome biology*, *25*(1), 67.

[40] Wang, S., Xing, H., Hua, C., Guo, H. S., & Zhang, J. (2016). An Improved Single-Step Cloning Strategy Simplifies the Agrobacterium tumefaciens-Mediated Transformation (ATMT)-Based Gene-Disruption Method for Verticillium dahliae. *Phytopathology*, *106*(6), 645–652.

[41] Chen, S., Zhou, Y., Chen, Y., & Gu, J. (2018). fastp: an ultra-fast all-in-one FASTQ preprocessor. *Bioinformatics (Oxford, England)*, *34*(17), i884–i890.

[42] Li, H. Aligning sequence reads, clone sequences and assembly contigs with BWA-MEM(2013). Preprint at https://doi.org/10.48550/arXiv.1303.3997.

[43] Danecek, P., Bonfield, J. K., Liddle, J., Marshall, J., Ohan, V., Pollard, M. O., Whitwham, A., Keane, T., McCarthy, S. A., Davies, R. M., & Li, H. (2021). Twelve years of SAMtools and BCFtools. *GigaScience*, *10*(2), giab008.

[44] Zhang, Y., Liu, T., Meyer, C. A., Eeckhoute, J., Johnson, D. S., Bernstein, B. E., Nusbaum, C., Myers, R. M., Brown, M., Li, W., & Liu, X. S. (2008). Model-based analysis of ChIP-Seq (MACS). *Genome biology*, *9*(9), R137.

[45] Kurtenbach, S. & Harbour, J. W. SparK: A Publication-quality NGS Visualization Tool(2019). 845529 Preprint at https://doi.org/10.1101/845529.

[46] Yu, G., Wang, L. G., & He, Q. Y. (2015). ChIPseeker: an R/Bioconductor package

for ChIP peak annotation, comparison and visualization. *Bioinformatics (Oxford, England)*, *31*(14), 2382–2383.

[47] Ramírez, F., Ryan, D. P., Grüning, B., Bhardwaj, V., Kilpert, F., Richter, A. S., Heyne, S., Dündar, F., & Manke, T. (2016). deepTools2: a next generation web server for deep-sequencing data analysis. *Nucleic acids research*, *44*(W1), W160–W165.

## Supplementary Materials:

Figure S1: *V. dahliae* V592 genome assembly presentation;
Figure S2: Genome-wide profiling of nonspecific IgG signals and histone modification patterns in *V. dahliae* using fCUT&Tag-seq;
Figure S3: Original images of Figure 2A, Figure 4A, Figure 7A;
Table S1: Primers used in this study.

## Author Contributions:

**H.W.**: methodology, investigation, data curation, formal analysis, writing-original draft, and writing—review and editing;
**Y.T.**: methodology, investigation, data curation, formal analysis, writing-original draft, and writing—review and editing;
**J.M.**: biostatistics analysis, data curation, writing-original draft, and writing—review and editing;
**J.Y.**: formal analysis, writing—original draft, and writing-review and editing;
**M.L.**: formal analysis, writing—original draft, and writing-review and editing;
**S.L.**: supervision, investigation, resources, data curation;
**H.X.**: methodology, investigation, data curation, finish the experiments involving *Fusarium graminearum*;
**G.T.**: methodology, investigation, data curation, finish the experiments involving *Fusarium graminearum*;
**W.L.**: supervision, methodology, data curation, finish the experiments involving *Fusarium graminearum*;
**H-S.G.**: supervision, project administration, methodology, resources, data curation, writing-review and editing.
**C-M.S.**: conceptualization, supervision, project administration, methodology, resources, data curation, writing-original draft, writing-review and editing.
All authors have read and agreed to the published version of the manuscript.

**Funding:**

This research was funded by the Chinese Academy of Sciences (CAS) Projects for Young Scientists in Basic Research (Grant no. YSBR-080), the Strategic Priority Research Program of Chinese Academy of Sciences (Grant no. XDA0450000) to C-M.S, and the Young Scientists Fund of the National Natural Science Foundation of China (Grant no. 32402338) to H.W.

Institutional Review Board Statement: Not applicable.

Informed Consent Statement: Not applicable.

Data Availability Statement: Data are contained within the article and Supplementary Materials.

**Acknowledgments:**

We thank Xiao Liu for providing *Neurospora crassa* strains. The work was supported by the Chinese Academy of Sciences (CAS) Projects for Young Scientists in Basic Research (Grant no. YSBR-080), the Strategic Priority Research Program of Chinese Academy of Sciences (Grant no. XDA0450000) to C-M.S., and the Young Scientists Fund of the National Natural Science Foundation of China (Grant no. 32402338) to H.W.

The funder has not played any role in the study design, data collection and analysis, the decision to publish, or the preparation of the manuscript.

**Conflicts of Interest:**

The authors declare that there is no conflict of interest.

A

| Sample | SeqNum | SumBase | N50Len | N90Len | MeanLen | MaxLen |
|---|---|---|---|---|---|---|
| *Verticillium dahliae* V592 | 156947206 | 40711754401 | 452 | 136 | 64.849 | 9518 |

B

| Chr | Chr1 | Chr2 | Chr3 | Chr4 | Chr5 | Chr6 | Chr7 | Chr8 |
|---|---|---|---|---|---|---|---|---|
| Length | 4416504 | 7834363 | 5191406 | 4182892 | 3710032 | 3337687 | 3268461 | 3754928 |
| GC% | 52.88 | 54.63 | 51.5 | 52.89 | 53.32 | 53.11 | 52.31 | 55.27 |

C

| Sample | Gene Number | CDS Averange length | CDS Averange GC(%) |
|---|---|---|---|
| Verticillium_dahliae_V592 | 8332 | 1435.8863 | 59.55 |

D

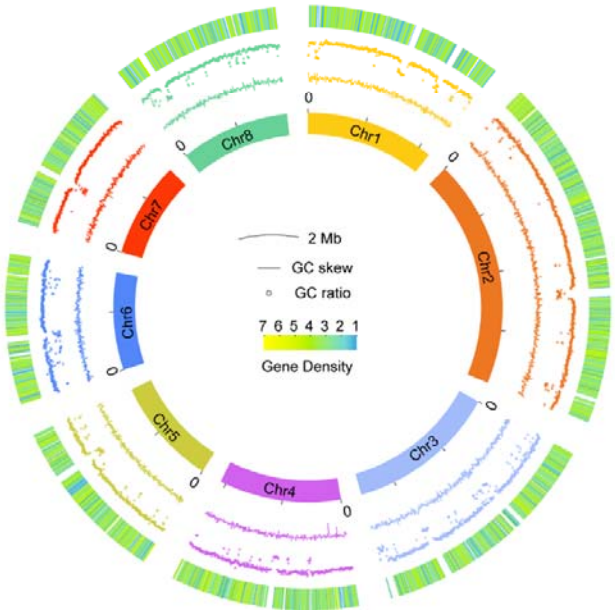


**Figure S1. *V. dahliae* V592 genome assembly presentation**

**A.** The output quality of sequencing data. Sample: sample name; SeqNum: number of sequences; SumBase: total number of data bases; N50Len: N50 length of sequencing data; N90Len: length of sequencing data N90; MeanLen: mean length of sequencing sequence; MaxLen: maximum length of sequencing sequence. **B.** Assembly result statistic. Length: length of the sequence after concatenation; GC (%): GC content of the concatenated sequence. **C.** The CIRCOS plot of the genome.

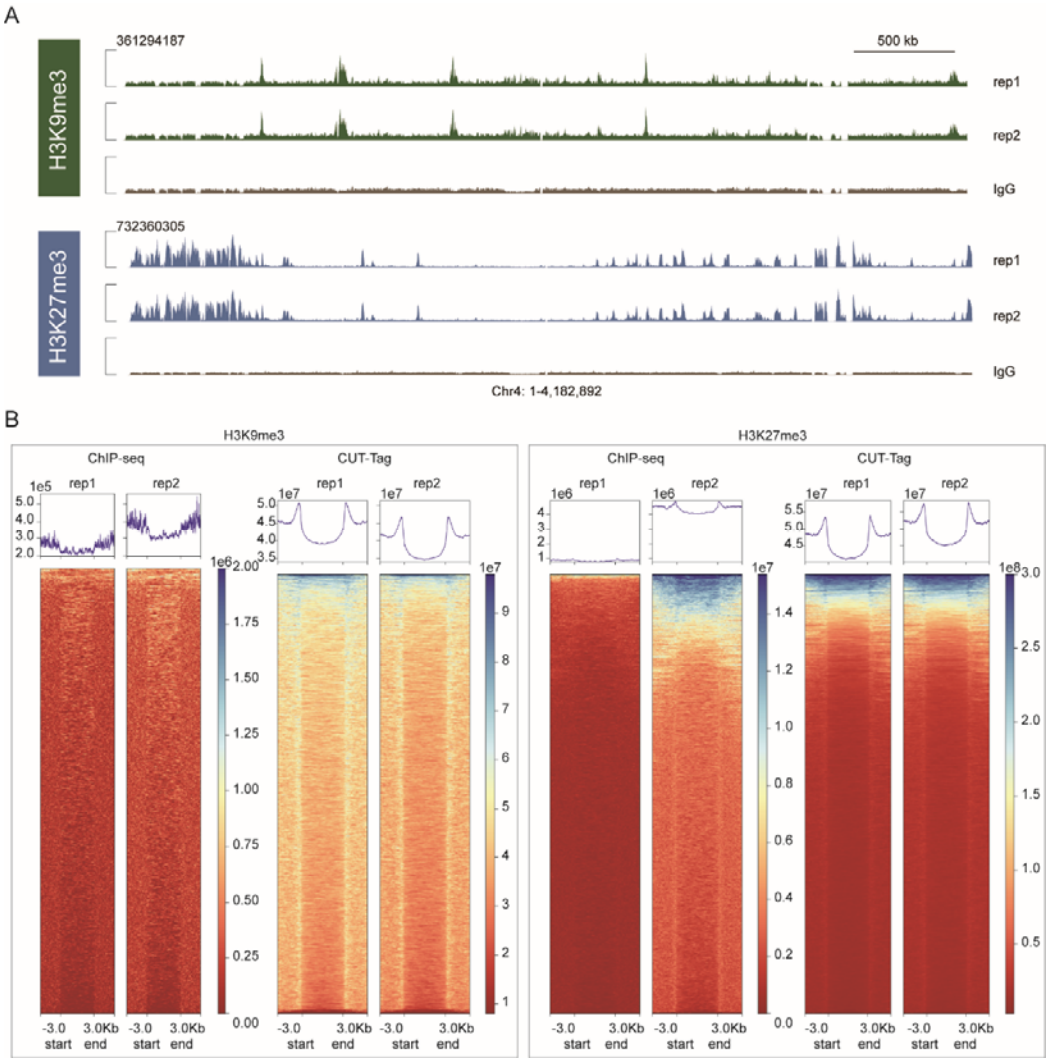


**Figure S2. Genome-wide profiling of nonspecific IgG signals and histone modification patterns in *V. dahliae* using fCUT&Tag-seq**

**A.** Genome browser view of the H3K9me3, H3K27me3, and nonspecific IgG antibody signals across representative genomic regions in Wild-type strain. The minimal background signal demonstrates the specificity of the fCUT&Tag-seq method. Data were presented at the same scale as specific antibody signals. **B.** Heatmap analysis of H3K9me3 and H3K27me3 signals near protein-coding genes in CUT&Tag-seq and ChIP-seq. Scale regions were 3,000 bp upstream of the translation starting site (TSS), 3,000 bp downstream of the translation end site (TES), and a 1,000-bp region on the gene body. The lengths were plotted using the computeMatrix and plotHeatmap tools in deepTools.

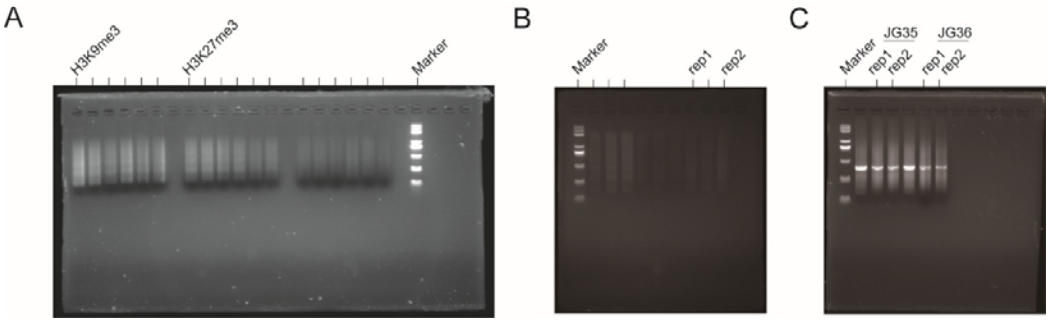


**Figure S3: Original images of Figure 2A, Figure 4A, Figure 7A**

**A.** Original images of Figure 2A. **B.** Original images of Figure 4A. **C.** Original images of Figure 7A